AD-A069 084 NAVAL RESEARCH LAB WASHINGTON D C F/G 11/6
IMPROVEMENT OF ENVIRONMENTAL CRACK PROPAGATION RESISTANCE IN TI--ETC(U)
MAR 79 G R YODER, L A COOLEY, T W CROOKER
UNCLASSIFIED NRL-MR-3955 SBIE-AD-E000 298 NL

| OF |
AD
A069 084

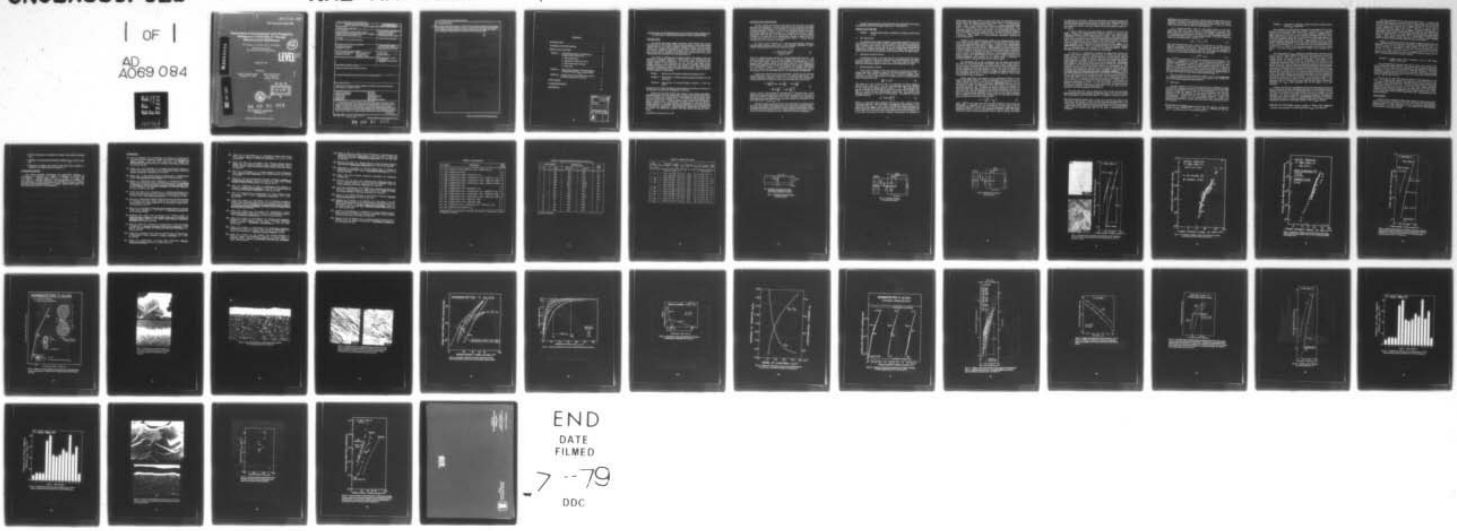

END
DATE
FILMED
-7 -79
DDC

NRL Memorandum Report 3955

Improvement of Environmental Crack Propagation Resistance in Ti–8Al–1Mo–1V Through Microstructural Modification

G. R. YODER, L. A. COOLEY, AND T. W. CROOKER

Metals Performance Branch
Material Science and Technology Division

March 19, 1979

Prepared for

Naval Air Systems Command
Washington, D.C. 20361

Office of Naval Research
800 N. Quincy St.
Arlington, VA 22217

NAVAL RESEARCH LABORATORY
Washington, D.C.

SECURITY CLASSIFICATION OF THIS PAGE (When Data Entered)

REPORT DOCUMENTATION PAGE

READ INSTRUCTIONS BEFORE COMPLETING FORM

1. REPORT NUMBER: NRL Memorandum Report 3955
2. GOVT ACCESSION NO.
3. RECIPIENT'S CATALOG NUMBER

4. TITLE (and Subtitle): IMPROVEMENT OF ENVIRONMENTAL CRACK PROPAGATION RESISTANCE IN Ti-8Al-1Mo-1V THROUGH MICROSTRUCTURAL MODIFICATION

5. TYPE OF REPORT & PERIOD COVERED: Final report on one phase of a continuing NRL problem.

6. PERFORMING ORG. REPORT NUMBER

7. AUTHOR(s): G.R. Yoder, L.A. Cooley, and T.W. Crooker

8. CONTRACT OR GRANT NUMBER(s)

9. PERFORMING ORGANIZATION NAME AND ADDRESS: Naval Research Laboratory, Washington, DC 20375

10. PROGRAM ELEMENT, PROJECT, TASK AREA & WORK UNIT NUMBERS: NRL Problems M01-24 and M01-53; RR 022-01 & Work Unit 1P7-113

11. CONTROLLING OFFICE NAME AND ADDRESS: Naval Air Systems Command, Washington, DC 20361; Office of Naval Research, 800 N. Quincy St., Arlington, VA 22217

12. REPORT DATE: March 19, 1979

13. NUMBER OF PAGES: 42

14. MONITORING AGENCY NAME & ADDRESS (if different from Controlling Office)

15. SECURITY CLASS. (of this report): UNCLASSIFIED

15a. DECLASSIFICATION/DOWNGRADING SCHEDULE

16. DISTRIBUTION STATEMENT (of this Report)

Approved for public release; distribution unlimited.

61153N

17. DISTRIBUTION STATEMENT (of the abstract entered in Block 20, if different from Report)

18. SUPPLEMENTARY NOTES

Prepared for Naval Air Systems Command, Washington, DC 20361 and Office of Naval Research, 800 N. Quincy St., Arlington, VA 22217.

19. KEY WORDS (Continue on reverse side if necessary and identify by block number)

Fatigue crack propagation	Beta anneal
Stress-corrosion cracking	Microstructure
Corrosion fatigue	Widmanstätten packets
Titanium alloys	Heat treatment
Duplex anneal	Microstructural modification

20. ABSTRACT (Continue on reverse side if necessary and identify by block number)

A study has been conducted to improve crack tolerance properties of Ti-8Al-1Mo-1V through microstructural modification. Alloy microstructure was modified relative to that associated with the currently used duplex anneal through variations in heat treatment. Measurements were made of (i) fatigue crack growth in air, (ii) stress-corrosion cracking in 3.5% aqueous sodium chloride solution, and (iii) corrosion-fatigue in 3.5% aqueous sodium chloride solution. Results indicate that relative to crack tolerance properties of the duplex-annealed microstructure, the beta-annealed Widmanstätten

(Continues)

DD FORM 1 JAN 73 1473 EDITION OF 1 NOV 65 IS OBSOLETE S/N 0102-014-6601

SECURITY CLASSIFICATION OF THIS PAGE (When Data Entered)

20. Abstract (Continued)

microstructure offers superior resistance on all three bases of comparison; specifically, a 40-fold improvement in fatigue crack growth resistance in ambient air, a doubling of stress-corrosion-cracking threshold, and a resistance to corrosion-fatigue which exceeds the fatigue crack growth resistance of the duplex anneal in ambient air. Micromechanistic interpretations are discussed as appropriate.

CONTENTS

IMPROVEMENT OF ENVIRONMENTAL CRACK PROPAGATION RESISTANCE IN Ti-8Al-1Mo-1V THROUGH MICROSTRUCTURAL MODIFICATION

INTRODUCTION

For aircraft gas turbine engine components which operate near ambient temperatures, the Ti-8Al-1Mo-1V alloy has been preferred to other high-strength titanium alloys on the basis of superior strength-to-density ratio and elastic modulus [1,2]. Though the susceptibility of this alloy to stress-corrosion cracking and corrosion-fatigue has long been recognized [3-8], engine components of this alloy (which must be operable in salt-water laden environments) still exhibit cracking problems associated with this susceptibility [1].

In an effort to alleviate such cracking problems, the present study was undertaken to optimize resistance to crack growth in the Ti-8Al-1Mo-1V alloy through microstructural modification. In this work, alloy microstructure was modified relative to that associated with the currently used duplex anneal, through variations in heat treatment (e.g., changes in annealing temperatures, quenching temperature, cooling rates, post-quench anneal). Then crack growth resistance was determined for the modified microstructures, relative to that for the duplex anneal, in three phases:

PHASE I : Improvement of fatigue crack growth resistance in air.

PHASE II : Improvement of stress-corrosion-cracking resistance in 3.5% salt water.

PHASE III : Improvement of corrosion-fatigue resistance in 3.5% salt water.

Results from the initial two phases were considered preliminary to selection of the optimized microstructure investigated in Phase III.

Results from this work indicate that, relative to the currently used duplex-annealed material, a 40-fold improvement in fatigue crack growth resistance (in air) is obtainable with a beta-annealed (Widmanstätten) microstructure, which provides a concomitant doubling of K_{Iscc}, the stress-corrosion-cracking threshold in 3.5% salt water. Furthermore, the results indicate that the corrosion-fatigue resistance of the beta-annealed microstructure in 3.5% salt water is actually superior to the fatigue crack growth resistance of the duplex-annealed microstructure in ambient air. Micromechanistic interpretation of results will be offered, with appropriate evidence from light optical and electron microscopy.

Note: Manuscript submitted January 15, 1979.

MATERIALS AND PROCEDURES

The alloy studied was received in the form of 25.4 mm thick α/β –rolled plate with the composition: Ti-7.8Al-1.0Mo-0.07Fe-0.11 O-0.015N-0.03C-0.0046H. Microstructural modifications were imparted to this alloy according to the heat-treatment schedules in Table I. Of the 15 heat treatments therein, the duplex anneal (DA) is given as heat treatment no. 1. Heat treatment nos. 2–6 involve a beta-quench (BQ) and nos. 7-11 a beta anneal (BA); no. 12 involves possible formation of α'' phase and no. 13, perhaps some retained β phase; no. 14 is an extended beta anneal and no. 15 a recrystallization anneal. A vacuum furnace was employed in all of the heat treatments.

To screen these materials for stress-corrosion-cracking resistance, cantilever-bend specimens were used, of the geometry illustrated in Fig. 1. Values of stress-intensity factor were computed as [9,10]

$$K = \frac{4.12\ M\ (\alpha^{-3} - \alpha^{3})^{1/2}}{(B\ B_N)^{1/2}\ W^{3/2}} \qquad (1)$$

where M = applied bending moment, B = gross thickness (24.5 mm), B_N = net section thickness (22.1 mm), W = specimen height (49.9 mm) and $\alpha = 1-a/W$ (a = initial crack length). Specimens were subjected to sustained load in 3.5% aqueous sodium chloride solution, as described in Ref. [3]. If no indication of failure was observed in 24 h, the load was increased by an amount corresponding to $\sim 2.5\ MPa \cdot m^{1/2}$ increase in K; this procedure was repeated until failure occurred. Estimates of the K_{Iscc} threshold for a given material were taken as the average of K at the failure load and K at the immediately preceding load.

Fatigue crack growth rates were determined in ambient air from compact tension specimens of 25.4 mm thickness and a TL crack orientation [11]. The specimen geometry, illustrated in Fig. 2, is of the WOL type with a half-height-to-width (h/W) ratio of 0.486; the stress-intensity calibration is given by [12]

$$K = \frac{P\sqrt{a}}{BW}\left[30.96 - 195.8\left(\frac{a}{W}\right) + 730.6\left(\frac{a}{W}\right)^2 - 1186.3\left(\frac{a}{W}\right)^3 + 754.6\left(\frac{a}{W}\right)^4\right] \qquad (2)$$

where P = load, a = crack length, B = thickness and W = width (64.8 mm). Crack lengths were measured optically on both faces of the specimen at 15X, with all data taken within the range, $0.26 \le a/W \le 0.62$. Specimens were subjected to cyclic tension-to-tension loading with a haversine waveform, a frequency of 5 Hz and a load ratio $R = P_{min}/P_{max} = 0.10$.

Corrosion fatigue crack growth rates were determined in circulating 3.5% salt water from compact tension specimens of the geometry illustrated in Fig. 3. The planar dimensions of this specimen are twice those of the specimen in Fig. 2. The thickness was an identical 25.4 mm. Again, specimens were tested at a load ratio of R = 0.10, but frequencies of both 5 Hz and 0.1 Hz were investigated.

Uniaxial tensile properties were determined from standard 12.8 mm diameter specimens with a 50.8 mm gage length and a T orientation [11].

RESULTS AND ANALYSIS

PHASE I : 40-Fold Improvement in Resistance to Fatigue Crack Growth in Air

A. The enhancement

The microstructures which correspond to the duplex anneal (H.T. no. 1) and beta anneal (H.T. no. 7) are shown in Fig. 4, together with respective logarithmic plots of fatigue crack growth rates (da/dN) as a function of stress-intensity range (ΔK). Clearly, at a given value of ΔK, the beta-annealed Widmanstätten microstructure exhibits the superior resistance to fatigue crack growth, with da/dN as much as 40–fold reduced from levels associated with the duplex anneal.

B. Agreement of data for the DA

As illustrated in Fig. 5, the da/dN data for the duplex anneal from Fig. 4 are in good agreement with those obtained from actual fan blades in the duplex-annealed condition, as reported in Ref. [2]. These same data from Fig. 4 also agree well with those obtained recently at Pratt and Whitney [13], cf. Fig. 6.

C. Micromechanistic rationale

Crack growth behavior of the beta-annealed microstructure exhibits a bilinear form with a transition evident at the stress-intensity range, ΔK_T = 31 MPa$\cdot m^{1/2}$. This behavior is illustrated in Fig. 7, which is comprised of data trend lines from Fig. 4. Each branch of the bilinear plot can be characterized in terms of the power law [14],

$$\frac{da}{dN} = C(\Delta K)^m, \qquad (3)$$

with values of C and m shown in Fig. 7 as determined by linear regression analysis of data from Fig. 4. For the hypotransitional region, the exponent m = 7.4, while for the hypertransitional region m = 4.7. The transition itself appears to correlate with the point at which the reversed (cyclic) plastic zone size, r_y^c, attains the mean Widmanstätten packet size, $\bar{\ell}_{WP}$ (which is the effective grain size for this type of microstructure). The zone size, computed according to [15–21]

$$r_y^c = 0.033 \left(\frac{\Delta K}{\sigma_y}\right)^2 \qquad (4)$$

where σ_y is the yield stress, amounts to 50 μm at ΔK_T. This is in quite reasonable agreement with quantitative metallographic determination of the mean packet size, $\bar{\ell}_{WP}$ = 60 μm. Thus, the growth rate behavior parallels that found in prior work [20,21] with Ti-6Al-4V, shown in Fig. 8, which illustrates the double-lobed shape of the plane strain cyclic plastic zone and the dimension, r_y^c. In this figure, an attempt is made to illustrate schematically the influence of

cyclic plastic zone size, relative to packet size, upon the development of the bilinear form of the fatigue crack growth rate plots found for the Widmanstätten alloys: Below the transition point, where $r_y^c < \bar{\ell}_{WP}$, a microstructurally sensitive mode of crack growth occurs which involves crystallographic bifurcation in Widmanstätten packets that border the Mode I crack plane. This bifurcation causes a reduction in the effective ΔK and consequently da/dN, as well as the appearance of the transition itself. By contrast, above the transition where $r_y^c > \bar{\ell}_{WP}$, the packets within the larger r_y^c must necessarily deform as a continuum, which results in a microstructurally insensitive, nonbifurcated mode of crack growth.

Contrast in the microstructurally sensitive and microstructurally insensitive modes of crack growth is illustrated for the beta-annealed Ti-8Al-1Mo-1V by the crack-path sectioning results in Fig. 9. Details of the crystallographic bifurcation exhibited in Fig. 9(a) are thought to parallel those already determined in the case of Ti-6Al-4V [19,20]. Metallographic crack-path sectioning of structure-insensitive crack growth in the case of the duplex anneal is illustrated in Fig. 10. Here, as in Fig. 9(b), the trace of the fracture surface is again flat, with no evidence of crystallographic bifurcation. In the scanning electron micrographs of Fig. 11, the relative flatness of the fracture surface associated with structure-insensitive crack growth for the duplex anneal is compared to structure-sensitive crack growth observed for the beta anneal.

The comparative plot in Fig. 12 illustrates that the fatigue crack growth rate data for the beta-annealed Ti-8Al-1Mo-1V (the "60 μm" alloy) serve to extend an effect determined earlier for Widmanstätten Ti-6Al-4V alloys [20,21], viz. the reduction in da/dN with increased $\bar{\ell}_{WP}$, as a 20 to 25-fold reduction in da/dN is observed for a 3.5-fold increase in $\bar{\ell}_{WP}$. This effect is attributed to the observation that bifurcated cracks in the crack tip region increase in size with increasing packet size, to thereby diminish the effective ΔK and thus reduce da/dN as $\bar{\ell}_{WP}$ is increased.

Though <u>mean</u> packet size appears to have predominant influence on the fatigue crack growth behavior of these Widmanstätten microstructures, as indicated in Fig. 12, the nature of the packet size <u>distribution</u> appears to have an important effect upon the shape of the fatigue crack growth rate plot, viz. that the spread in packet size distribution of an alloy affects the sharpness of transition observed at ΔK_T. To examine this effect in quantitative fashion, it is first noted that since both branches of the bilinear growth-rate plot obey the power law of Eq. (3), the sharpness of transition can be indexed as the ratio of hypo to hypertransitional exponents, $m_B{:}m_A$, which can be readily computed. Next, the degree of clustering of packet sizes about the mean value for a given alloy is computed from the data in Fig. 13 as [21]

$$\gamma \equiv (\ell_{WP}^{0.95} - \bar{\ell}_{WP})^{-1} \qquad (5)$$

where $\ell_{WP}^{0.95}$ is the packet size from the 95th percentile of the packet size distribution, as illustrated for the Ti-8Al-1Mo-1V (60 μm) alloy in Fig. 13. (Schematic illustration is made in Fig. 14 of the difference in clustering for two hypothetical alloys, X and Y, with significantly different packet size distributions.) For the five alloys represented in Fig. 12, values of $m_B{:}m_A$ are plotted

as a function of γ in Fig. 15. Clearly, the sharpness of transition increases with increased clustering of packet sizes about the mean value. Perhaps this point is best illustrated, however, with reference to Fig. 16, where da/dN vs. ΔK data are compared for three of the alloys, together with their respective values of and m_B:m_A.

In Fig. 15, values of m_A are also plotted as a function of γ for the five alloys. Clearly, the hypertransitional exponents appear to decrease with increased clustering of packet sizes about the mean. This effect appears attributable to a remnant of microstructurally sensitive crack growth which occurs in the nominally structure-insensitive, hypertransitional region modeled in Fig. 8. The significance of such a remnant would obviously diminish as clustering increases, thereby providing fewer packets to meet the condition, $\ell_{WP} > r_y^c > \bar{\ell}_{WP}$, necessary for any remnant of structure-sensitive crack growth in the hypertransitional region. Thus as clustering increases, the transition sharpens and m_A decreases since any remnant of the structure-sensitive, crystallographically bifurcated mode of crack growth is diminished.

At this point, it is appropriate to address the displacement between the fatigue crack growth resistance associated with the duplex and beta anneals, which amounts to as much as a 40-fold difference in crack growth rates, as illustrated in Fig. 4. Though the basis for microstructural dependence of fatigue crack propagation resistance in titanium alloys has been poorly understood, a breakthrough on this subject appears to have just emerged [22]: Specifically, from studies of a wide variety of materials from the Ti-6Al-4V, Ti-6Al-6V-2Sn, Ti-8Al-1Mo-1V and Ti-6Al-2Cb-1Ta-0.8Mo systems (as distinguished by compositional variations and heat treatment), we have observed a 50–fold difference in fatigue crack propagation resistance which is traceable to a grain-size effect, with larger grain size associated with better propagation resistance. In brief, the 50-fold difference in da/dN (observed at $\Delta K = 21$ MPa$\cdot$m$^{1/2}$) is illustrated in Fig. 17, with growth rates for the duplex annealed and beta annealed Ti-8Al-1Mo-1V near both extremes of the da/dN data band. The material growth rates at $\Delta K = 21$ MPa$\cdot$m$^{1/2}$ are plotted in Fig. 18 as a function of mean grain size ($\bar{\ell}$), which varies some 15–fold between the different materials*. Clearly, there is a systematic dependence of da/dN on $\bar{\ell}$, such that fatigue crack growth rates decrease with increased grain size. Of prime significance, the duplex-annealed Ti-8Al-1Mo-1V exhibits a much smaller grain size, $\bar{\ell} = 9$ μm, than the 60 μm associated with the beta-annealed Ti-8Al-1Mo-1V.

This grain-size effect can be explained in terms of the reversed (cyclic) plastic zone size model, by extension of principles already evolved in our studies with Widmanstätten microstructures [18–21]. To begin, it is assumed that the

*The linear intercept measurements of grain size reported here relate to the grain size of the primary α phase for microstructures associated with a mill anneal (MA), recrystallization anneal (RA) or duplex anneal (DA); in the case of a beta anneal (BA), grain-size measurements relate to the Widmanstätten packet size, the effective grain size for this class of microstructures [18, 19,23-25].

logarithmic plot of da/dN vs. ΔK for a material of given mean grain size (but otherwise of arbitrary microstructural type) exhibits a bilinear form with a transition at "T," sketched in Fig. 19 (solid lines), such that at ΔK_T, the reversed plastic zone size (cf. Eq. 4) attains the mean grain size.*

If a structure-sensitive mode of crack growth occurs in the hypotransitional region II.a, which involves a crystallographic bifurcation, then growth rates vary inversely with mean grain size (owing to larger bifurcations with increased mean grain size); by contrast, in the hypertransitional region II.b, a structure-insensitive mode of crack growth occurs. If Eq. (4) is rewritten relative to the transition point, where $r_y^c = \bar{\ell}$,

$$\Delta K_T = 5.5\, \sigma_y \bar{\ell}^{1/2} \qquad (6)$$

then, with increased grain size, a shift in the data plot to the right is to be expected, as sketched in Fig. 19 (cf. dashed lines) and observed for Widmanstätten microstructures (cf. Fig. 12). Consider further that the sharpness of transition, as well as hypertransitional slope itself, is influenced by the degree of clustering of the grain-size distribution about the mean value

$$\gamma = (\ell^{0.95} - \bar{\ell})^{-1} \qquad (7)$$

where $\ell^{0.95}$ is the grain size from the 95th percentile of the distribution. This behavior is attributable to a remnant of structure-sensitive growth in the nominally hypertransitional region II.b, owing to grains in excess of the mean value, $\bar{\ell}$. Consequently, even in the hypertransitional region II.b of Fig. 19, a lower growth rate can be anticipated for the material of larger $\bar{\ell}$ at a given ΔK (II.b), i.e., a lower da/dN at point Y than at point X, owing to a larger remnant of structure-sensitive growth by virtue of closer proximity to the transition point in the case of the former, all other factors being equal (including γ).

Thus the grain-size effect observed in Figs. 17 and 18 is comprehensible, even though the crack growth rates for many of the alloys at $\Delta K = 21$ MPa$\cdot$m$^{1/2}$ are in the nominally hypertransitional region II.b.

D. Other data

For heat treatment no. 13, Fig. 20 indicates that the resistance to fatigue crack growth is marginally superior to even that associated with the beta anneal, over most of the spectrum of ΔK levels for which comparison can be made. Preliminary evidence [26] suggests that the low-cycle-fatigue crack initiation resistance of this microstructure is significantly better than for the other microstructures. Further work will be required, however, to resolve the micromechanistic behavior of this microstructure, which may involve some transformation plasticity as Gilmore and Imam [27,28] have reported in the Ti-6Al-4V system.

*In the case of the duplex-annealed Ti-8Al-1Mo-1V (cf. Fig. 4), a transition is evident at $\Delta K_T \approx 16$ MPa$\cdot$m$^{1/2}$. By Eq. 4, with $\sigma_y = 958$ MPa for the DA, $r_y^c \approx 9\ \mu$m, the same as $\bar{\ell}$ for this microstructure.

PHASE II : Concomitant Doubling of Stress-Corrosion Cracking Threshold (K_{Iscc}) in Salt Water

The resistance to stress-corrosion cracking, as determined for all 15 heat treatments, is summarized in Table 2 and Fig. 21. Levels of the K_{Iscc} threshold range from 24.1 to 61.2 MPa•$m^{1/2}$, with the worst resistance associated with the duplex anneal (H.T. no. 1) and the best resistance associated with heat treatments which include an anneal above the beta transus. Heat treatment nos. 7-11 of the beta anneal (BA) family, give levels of K_{Iscc} (41.3-48.0 MPa•$m^{1/2}$) which are approximately double that of the DA.* Heat treatment nos. 12-14, which include a preliminary anneal above the beta transus, similarly provide high levels of K_{Iscc} (43.8-61.2 MPa•$m^{1/2}$). On the other hand, the recrystallization anneal (RA) of H.T. no. 15 (which did not involve an anneal above the beta transus) provides a low level of K_{Iscc} (26.7 MPa•$m^{1/2}$) similar to that observed for the DA.

The improvement in K_{Iscc} obtained by annealing above the beta transus (i.e. H.T. nos. 6-14) relative to the DA (and RA) can be rationalized in terms of a textural change. Since there is an excellent correlation between Young's modulus (E) and the degree of preferred orientation of basal planes in the α-phase [29-31], the textural change can be described with reference to the modulus data presented in Table 3. For the DA (H.T. no. 1), the values of E (136 and 125 GPa in the T and L directions, respectively) indicate a strong transverse texture in the plate material, with basal planes preferentially oriented parallel to the Mode I crack plane for the TL crack orientation in which all of the K_{Iscc} data were taken. Thus, the low resistance to stress-corrosion cracking is to be expected [8]. For the BA (H.T. no. 7), however, values of E (128 GPa in both the T and L directions) indicate that the basal pole density has been equilibrated between the T and L directions (and thus for the TL and LT crack orientations), as has been observed in prior work [20,21,29]. In other words, it might be said that the BA has served to "wash out" the original transverse texture. Consequently, with the opportunity for basal plane stress-corrosion susceptibility diminished, the K_{Iscc} values associated with the BA appear to be much enhanced.

Evidence obtained from metallographic crack path sectioning normal to the Mode I crack plane reveals a significant difference in stress-corrosion behavior associated with the BA and DA, as illustrated in Fig. 22. In the case of the DA, the trace of the Mode I crack plane is quite flat, with no evidence of crack bifurcation. For the BA, by contrast, the crack path exhibits a high degree of tortuosity, with massive evidence of crystallographic bifurcation. Presumably, such bifurcation serves to reduce the effective stress-intensity factor, and as a consequence, promote the much higher apparent level of K_{Iscc} threshold.

*For H.T. no. 7, for which extensive analysis of fatigue crack propagation resistance was described in the preceding section, K_{Iscc} = 42.6 MPa•$m^{1/2}$.

For heat treatments of the beta quench (BQ) family, it is unclear that significant enhancement of stress-corrosion-cracking resistance can be obtained relative to that observed for the DA, as K_{Iscc} levels for H.T. nos. 2-6 lie near both extremes of the threshold data in Table 2 and Fig. 21. On the basis of textural considerations, high levels of K_{Iscc} would be anticipated, since an anneal above the beta transus was performed. However, and perhaps most importantly, severe residual stress problems associated with the water quench could also be anticipated. It is thus thought that the somewhat contradictory nature of results for the BQ family may be attributable to residual quench stresses. (Such residual stresses may have led to problems with obtaining uniform precrack fronts, as noted in Table 2 for H.T. nos. 5 and 6.)

Finally, it is useful to consider the tradeoffs between strength level and K_{Iscc} threshold for the different heat treatments, as illustrated in Fig. 23. In particular, note that the ultimate tensile strength of the BA, H.T. no. 7 ($\sigma_{UTS} \approx 898$ MPa), is diminished some 11% from the level associated with the DA, H.T. no. 1 ($\sigma_{UTS} \approx 1006$ MPa), while the K_{Iscc} resistance of the BA is 77% higher and the da/dN resistance of the BA some 4000% greater than for the DA. Other mechanical properties are shown in Table 3.

PHASE III : Fatigue Crack Growth Resistance of BA in Salt Water Superior to DA in Air

For microstructures associated with the BA (H.T. no. 7) and DA (H.T. no. 1), fatigue crack growth rates in 3.5% aqueous sodium chloride solution are plotted in Fig. 24. Data trend lines (dashed) for the respective crack growth resistance in ambient air are also shown to facilitate comparison. Of prime significance, growth rates for the BA in salt water (at 5 Hz) are approximately an order of magnitude less than those for the DA in salt water, and even 4-fold less than those for the DA in air.

For the DA, the salt water data are shown for two frequencies, 0.1 and 5 Hz. The marginally lower growth rates observed at 0.1 Hz over much of the ΔK spectrum may possibly reflect a frequency inversion effect similar to that reported by Dawson and Pelloux [32]. An attempt was also made to determine crack growth resistance for the BA at 0.1 Hz in salt water. Though preliminary indications were that growth rates were less than observed at 5 Hz, unfortunately the crack deviated significantly from the Mode I crack plane at 0.1 Hz, so as to render data invalid by ASTM Method E647-78T. (Consequently, the test was discontinued.)

CONCLUSIONS

Results of this investigation indicate that through microstructural modification, crack tolerance properties of the Ti-8Al-1Mo-1V alloy can be significantly improved relative to those associated with the conventional duplex-annealed microstructure. Of prime importance, it was found that the beta-annealed, Widmanstätten microstructure offers:

- 40-fold improvement in resistance to fatigue crack growth in ambient air; a
- Doubling of stress-corrosion-cracking threshold (K_{Iscc}) in salt water; and
- Resistance to fatigue crack growth in salt water that is superior to resistance of the duplex anneal in ambient air.

ACKNLOWLEDGMENTS

The authors gratefully acknowledge the experimental assistance of F. D. Bogar, R. L. Newbegin, M. L. Cigledy, G. W. Jackson, C. R. Forsht and T. R. Harrison. Special thanks are due C. T. Fujii, F. D. Bogar and R. W. Judy, Jr., for helpful discussions. The encouragement of J. M. Krafft is also appreciated. This work was supported by the Naval Air Systems Command, under the stimulating directorship of R. J. Belisle. Supplementary support was also rendered by the Office of Naval Research.

REFERENCES

[1] Lee, E.U., Mahorter, R.G., and Wacaser, J.D., "Fracture of Ti-8Al-1Mo-1V Fan Blade by Stress Corrosion Cracking and Fatigue," in Fractography in Failure Analysis, ASTM STP 645, Edited by B.M. Strauss and W.H. Cullen, Jr., American Society for Testing and Materials, Philadelphia, PA, 1978, pp. 128–143.

[2] Cullen, W.H., and Stonesifer, F.R., "Fatigue-Crack-Growth Analysis of Titanium Gas-Turbine Fan Blades," NRL Memorandum Report 3378, Naval Research Laboratory, Washington, DC, Oct. 1976.

[3] Brown, B.F., "A New Stress-Corrosion Cracking Test for High-Strength Alloys," Materials Research and Standards, Vol. 6, 1966, pp. 129–133.

[4] Sandoz, G., "Subcritical Crack Propagation in Ti-8Al-1Mo-1V Alloy in Organic Environments, Salt Water, and Inert Environments," in Proceedings of Conference - Fundamental Aspects of Stress Corrosion Cracking, Edited by R.W. Staehle et al., National Association of Corrosion Engineers, Houston, TX, 1969, pp. 684–690.

[5] Curtis, R.E., Boyer, R.R., and Williams, J.C., "Relationship Between Composition, Microstructure, and Stress Corrosion Cracking (in Salt Solution) in Titanium Alloys," ASM Transactions Quarterly, Vol. 62, 1969, pp. 457-469.

[6] Bucci, R.J., "Environment Enhanced Fatigue and Stress Corrosion Cracking of a Titanium Alloy Plus a Simple Model for the Assessment of Environmental Influence on Fatigue Behavior," Ph.D. dissertation, Lehigh University, Bethlehem, PA, 1970.

[7] Meyn, D.A., "An Analysis of Frequency and Amplitude Effects on Corrosion Fatigue Crack Propagation in Ti-8Al-1Mo-1V," Metallurgical Transactions, Vol. 2, 1971, pp. 853–865.

[8] Blackburn, M.J., Smyrl, W.H., and Feeney, J.A., "Titanium Alloys," in Stress-Corrosion Cracking in High Strength Steels and in Titanium and Aluminum Alloys, Edited by B.F. Brown, Naval Research Laboratory, Washington, DC, 1972, pp. 245–363.

[9] Kies, J.A., Smith, H.L., Romine, H.E., and Bernstein, H., "Fracture Testing of Weldments," in Fracture Toughness Testing and its Applications, ASTM STP 381, American Society for Testing and Materials, Philadelphia, PA, 1965, pp. 328-353.

[10] Freed, C.N., and Krafft, J.M., "Effect of Side Grooving on Measurements of Plane-Strain Fracture Toughness," Journal of Materials, Vol. 1, 1966, pp. 770–790.

[11] Goode, R.J., "Identification of Fracture Plane Orientation," Materials Research and Standards, Vol. 12, No. 9, Sept. 1972, p. 31.

[12] Clark, W.G., Jr., and Hudak, S.J., Jr., "Variability in Fatigue Crack Growth Rate Testing," Journal of Testing and Evaluation, Vol. 3, No. 6, 1975, pp. 454–476.

[13] Beyer, J.R., Sims, D.L., and Wallace, R.M., "Titanium Damage Tolerant Design Data for Propulsion Systems," Report AFML-TR-77-101, Pratt & Whitney Aircraft Group, Government Products Division, West Palm Beach, FL, June 1977.

[14] Paris, P.C., and Erdogan, F., "A Critical Analysis of Crack Propagation Laws," Journal of Basic Engineering, Trans. ASME, Series D, Vol. 85, 1963, pp. 528–533.

[15] Paris, P.C., "The Fracture Mechanics Approach to Fatigue," in Fatigue -An Interdisciplinary Approach, Edited by J.J. Burke, N.L. Reed and V. Weiss, Syracuse University Press, Syracuse, NY, 1964, pp. 107-127.

[16] Rice, J.R., "Mechanics of Crack Tip Deformation and Extension by Fatigue," in Fatigue Crack Propagation, ASTM STP 415, American Society for Testing and Materials, Philadelphia, PA, 1967, pp. 247-309.

[17] Hahn, G.T., Hoagland, R.G., and Rosenfield, A.R., "Local Yielding Attending Fatigue Crack Growth," Metallurgical Transactions, Vol. 3, 1972, pp. 1189–1202.

[18] Yoder, G.R., Cooley, L.A., and Crooker, T.W., "A Transition to Enhanced Fatigue Crack Propagation Resistance in a β -Annealed Ti-6Al-4V Alloy of Commercial Purity," Proceedings of the Second International Conference on Mechanical Behavior of Materials, American Society for Metals, Metals Park, OH, 1976, pp. 1010–1014.

[19] Yoder, G.R., Cooley, L.A., and Crooker, T.W., "Observations on Microstructurally Sensitive Fatigue Crack Growth in a Widmanstätten Ti-6Al-4V Alloy," Metallurgical Transactions A, Vol. 8A, 1977, pp. 1737-1743.

[20] Yoder, G.R., Cooley, L.A., and Crooker, T.W., "Fatigue Crack Propagation Resistance of Beta-Annealed Ti-6Al-4V Alloys of Differing Interstitial Oxygen Contents," Metallurgical Transactions A, Vol. 9A, 1978, pp. 1413-1420.

[21] Yoder, G.R., Cooley, L.A., and Crooker, T.W., "Quantitative Analysis of Microstructural Effects on Fatigue Crack Growth in Widmanstätten Ti-6Al-4V and Ti-8Al-1Mo-1V," Engineering Fracture Mechanics, in press.

[22] Yoder, G.R., Cooley, L.A., and Crooker, T.W., "50-Fold Difference in Region–II Fatigue Crack Propagation Resistance of Titanium Alloys: A Grain-Size Effect," Journal of Engineering Materials and Technology, Trans. ASME, in press.

[23] Eylon, D., Hall, J.A., Pierce, C.M., and Ruckle, D.L., "Microstructure and Mechanical Properties Relationships in the Ti-11 Alloy at Room and Elevated Temperatures," Metallurgical Transactions A, Vol. 7A, Dec. 1976, pp. 1817–1826.

[24] Eylon, D., and Hall, J.A., "Fatigue Behavior of Beta Processed Titanium Alloy IMI 685," Metallurgical Transactions A, Vol. 8A, 1977, pp. 981–990.

[25] Shechtman, D., and Eylon, D., "On the Unstable Shear in Fatigued β-Annealed Ti-11 and IMI-685 Alloys," Metallurgical Transactions A, Vol. 9A, 1978, pp. 1018–1020.

[26] Krafft, J.M., Naval Research Laboratory, Washington, DC, unpublished research, 1978.

[27] Gilmore, C.M., and Imam, M.A., "Microstructure of Solution Treated Ti-6Al-4V," Technical Report No. III (B), Contract No. N00019-76-C-0136, The George Washington University, Washington, DC, Aug. 1976.

[28] Imam, M.A., and Gilmore, C.M., "Fatigue Life in Annealed and Martensitic Ti-6Al-4V," Technical Report No. II(B), Contract No. N00019-75-C-0093, The George Washington University, Washington, DC, Aug. 1975.

[29] Bowen, A. W., "Texture Stability in Heat Treated Ti-6Al-4V," Materials Science and Engineering, Vol. 29, 1977, pp. 19-28.

[30] Harrigan, M. J., Sommer, A. W., Reimers, P. G., and Alers, G. A., "The Effect of Rolling Texture on the Fracture Mechanics Properties of Ti-6Al-2Sn-4Zr-6Mo Alloy," in Titanium Science and Technology, Edited by R. I. Jaffee and H. M. Burte, Vol 2, TMS-AIME, Plenum Press, New York, NY, 1973, pp. 1297-1320.

[31] Larson, F., and Zarkades, A., "Properties of Textured Titanium Alloys," Report MCIC-74-20, Metals and Ceramics Information Center, Battelle-Columbus Laboratories, Columbus, OH, June 1974.

[32] Dawson, D. B., and Pelloux, R. M., "Corrosion Fatigue Crack Growth of Titanium Alloys in Aqueous Environments," Metallurgical Transactions, Vol. 5, 1974, pp. 723-731.

TABLE 1. Heat Treatments

No.	Type	Specification*	NRL Code
1	DA	(913°C/1 h + AC) + (579°C/8 h + AC) + (538°C/2 h + AC)	1
2	BQ	(1093°C/1/2 h + WQ)	2.a
3	BQ	(1093°C/1/2 h + WQ) + (816°C/1 h + AC)	2.b
4	BQ	(1093°C/1/2 h + WQ) + (1010°C/1/2 h + AC) + (816°C/1 h + AC)	2.c
5	BQ	(1093°C/1/2 h + WQ) + (1010°C/1/2 h + AC) + (816°C/1 h + WQ)	2.d
6	BQ	(1093°C/1/2 h + WQ) + (1010°C/1/2 h + WQ) + (816°C/1 h + WQ)	2.e
7	BA	(1093°C/1/2 h + AC)	3.a
8	BA	(1093°C/1/2 h + AC) + (816°C/1 h + AC)	3.b
9	BA	(1093°C/1/2 h + AC) + (1010°C/1/2 h + AC) + (816°C/1 h + AC)	3.c
10	BA	(1093°C/1/2 h + AC) + (1010°C/1/2 h + AC) + (816°C/1 h + WQ)	3.d
11	BA	(1093°C/1/2 h + AC) + (1010°C/1/2 h + WQ) + (816°C/1 h + WQ)	3.e
12	A″	(1093°C/1/2 h + AC) + (921°C/1 h + WQ)	4
13	RB	(1093°C/1/2 h + AC) + (849°C/2 h + WQ)	5
14	d_B	(1093°C/6 h + AC) + (1093°C/6 h + AC) + (816°C/1 h + AC)	6
15	RA	982°C/6 h + FC to 816°C + AC	7

*Anneals performed in vacuum furnace; h = hour, WQ = water quench, FC = furnace cool, AC = cooled in He @ approx. air cooling rate

TABLE 2. Thresholds for Stress-Corrosion Cracking (K_{Iscc})

Heat Treatment		Estimated K_{Iscc}		NRL Code
No.	Type	$MPa \cdot m^{1/2}$	$ksi \cdot in.^{1/2}$	
1	DA	24.1	21.9	1
2	BQ	26.0	23.7	2.a
3	BQ	26.0	23.7	2.b
4	BQ	25.9	23.6	2.c
5	BQ	(55.2	50.2)*	2.d
6	BQ	(60.1	54.7)*	2.e
7	BA	42.6	38.8	3.a
8	BA	41.3	37.6	3.b
9	BA	43.0	39.1	3.c
10	BA	(48.0	43.7)*	3.d
11	BA	45.6	41.5	3.e
12	A"	61.2	55.7	4
13	RB	43.8	39.9	5
14	d_B	50.8	46.2	6
15	RA	26.7	24.3	7

*questionable crack front

TABLE 3. Mechanical Properties

Heat Treatment		Orient.	0.2% Yield Strength, σ_y		Tensile Strength, σ_{uts}		$\frac{\sigma_{uts}}{\sigma_y}$	Strain Hard. Exp., n	% R.A.	% El.	Young's Modulus, E		NRL Code
No.	Type												
			MPa	ksi	MPa	ksi					GPa	10^3ksi	
1	DA	T	958	139	1025	149	1.07	0.036	20	13	136	19.7	1
		L	943	138	986	143	1.05	0.025	21	14	125	18.1	
5	BQ	T	840	122	952	138	1.13	0.054	13	11	125	18.1	2.d
6	BQ	T	862	125	958	139	1.11	0.049	16	10	123	17.8	2.e
7	BA	T	794	115	894	130	1.13	0.052	21	11	128	18.5	3.a
		L	803	116	901	131	1.12	0.052	20	12	128	18.5	
8	BA	T	818	119	895	130	1.09	0.043	18	10	125	18.1	3.b
9	BA	T	818	119	898	130	1.10	0.045	19	10	128	18.5	3.c
10	BA	T	809	117	898	130	1.11	0.049	19	10	120	17.4	3.d
11	BA	T	829	120	933	135	1.12	0.052	19	9	128	18.6	3.e
12	A″	T	774	112	942	137	1.22	0.074	19	10	119	17.2	4
13	RB	T	809	117	905	131	1.12	0.050	20	10	117	17.0	5
14	d_B	T	809	117	885	128	1.09	0.043	20	8	121	17.6	6

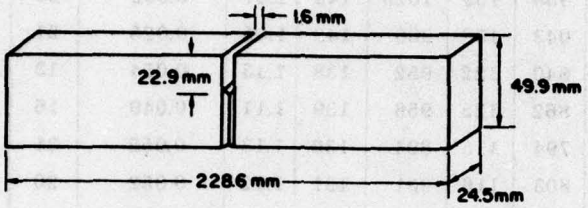

NOTE – NOTCH ROOT: 30° INCLUDED ANGLE, 0.076 mm ROOT RADIUS, SIDE GROOVE 45° INCLUDED ANGLE, 0.254 mm ROOT RADIUS, 1.2 mm DEPTH

Fig. 1 — Geometry of stress-corrosion-cracking specimen

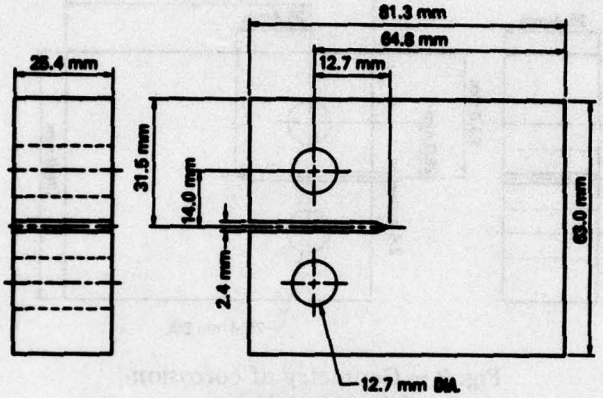

Fig. 2 — Geometry of fatigue crack growth specimen

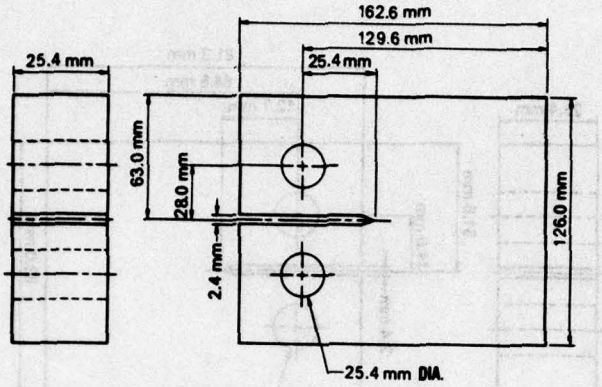

Fig. 3 — Geometry of corrosion-fatigue specimen

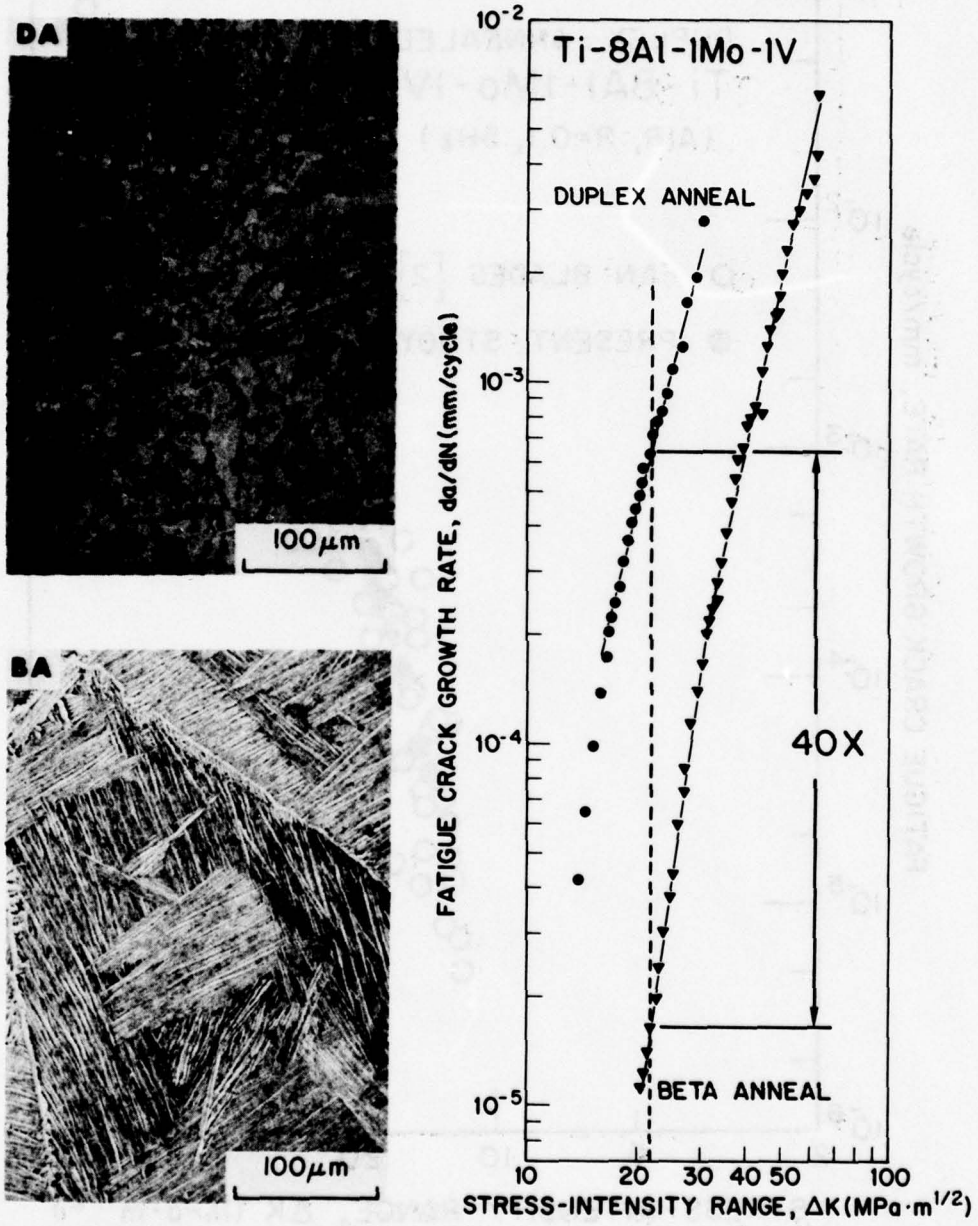

Fig. 4 — Microstructures and fatigue crack growth rates for the duplex anneal (DA) and beta anneal (BA) in room temperature air, with R = 0.1 and ν = 5 Hz

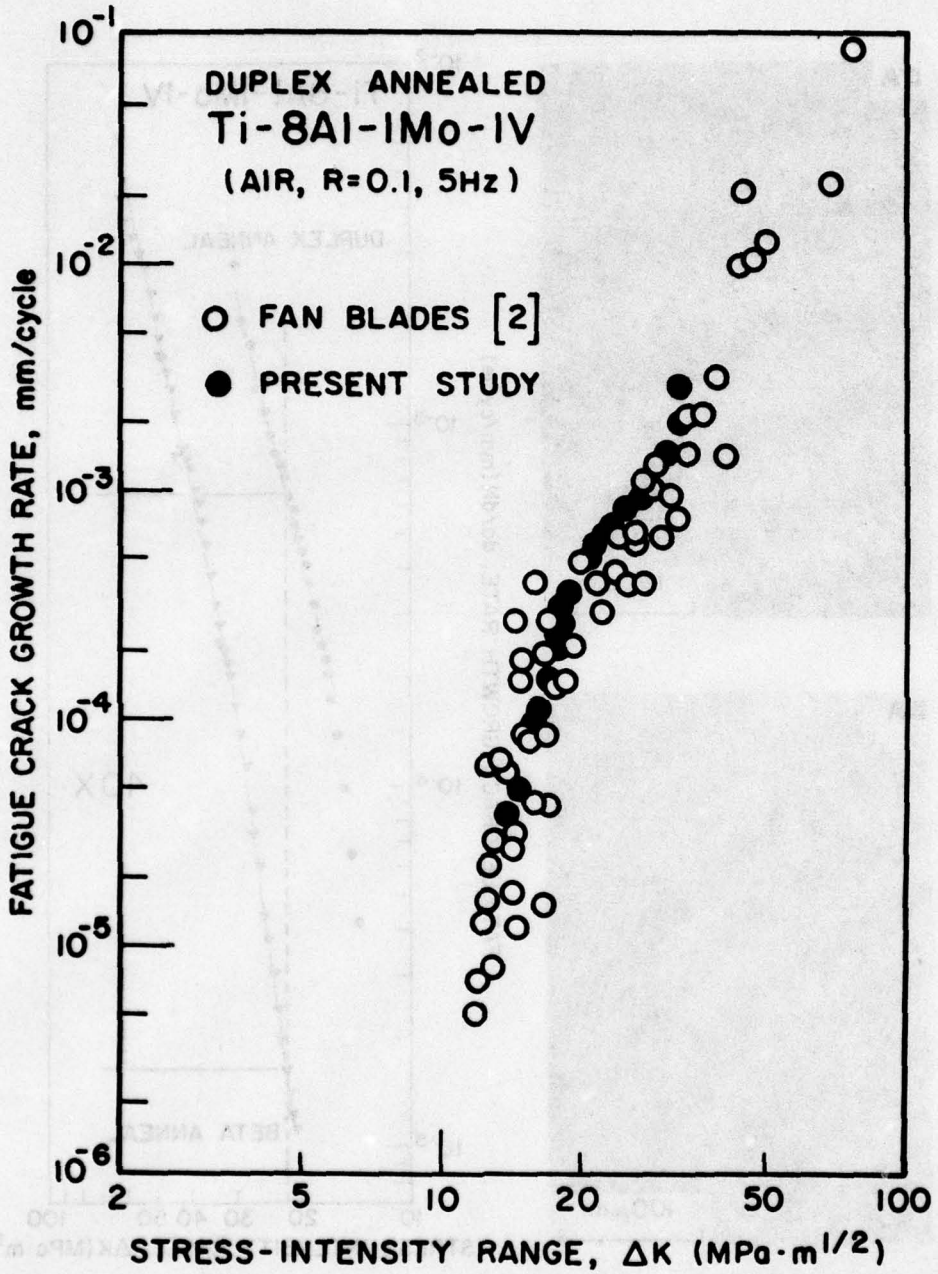

Fig. 5 — Comparison of fatigue crack growth rates for the duplex anneal to those from actual fan blades [2]

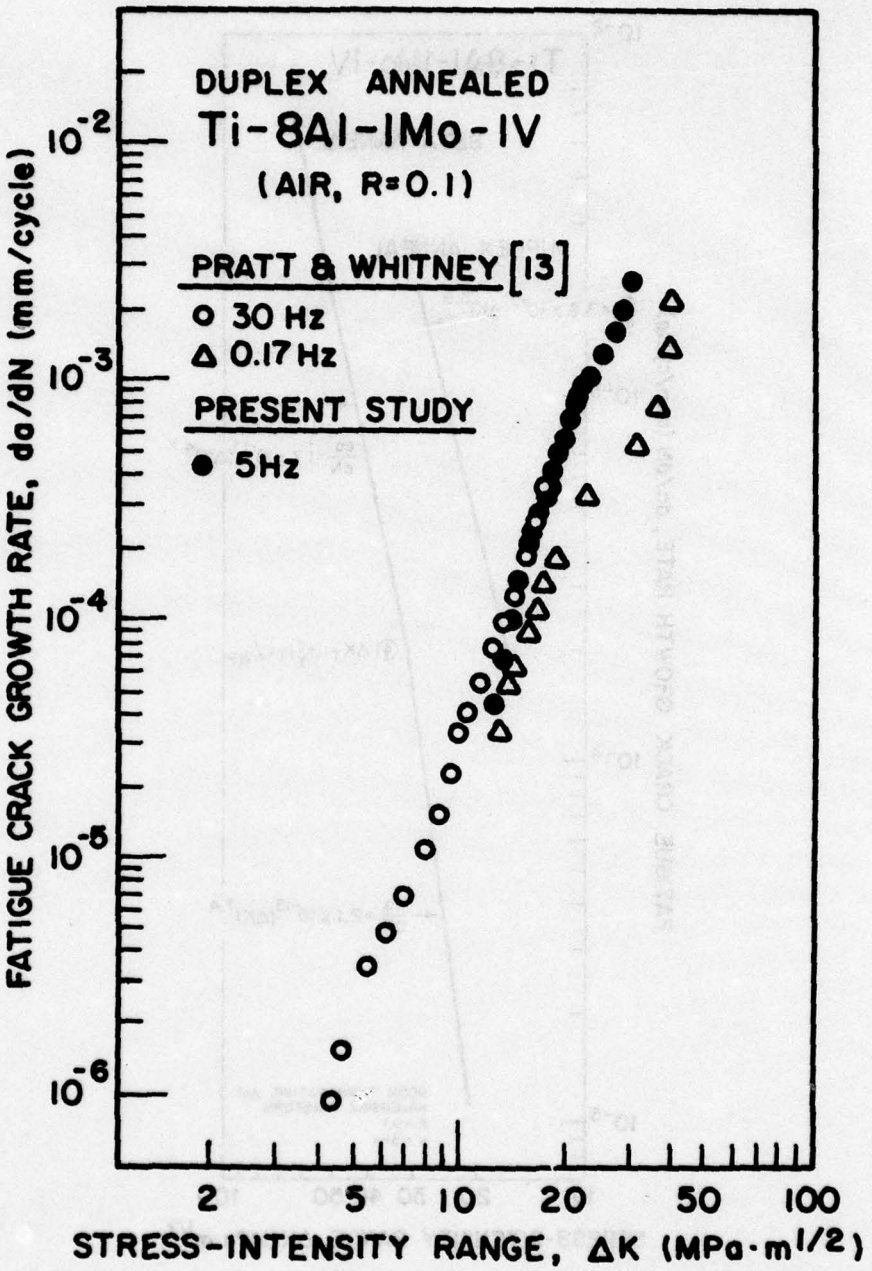

Fig. 6 — Comparison of fatigue crack growth rates for the duplex anneal obtained in the present study to those determined at Pratt and Whitney [13]

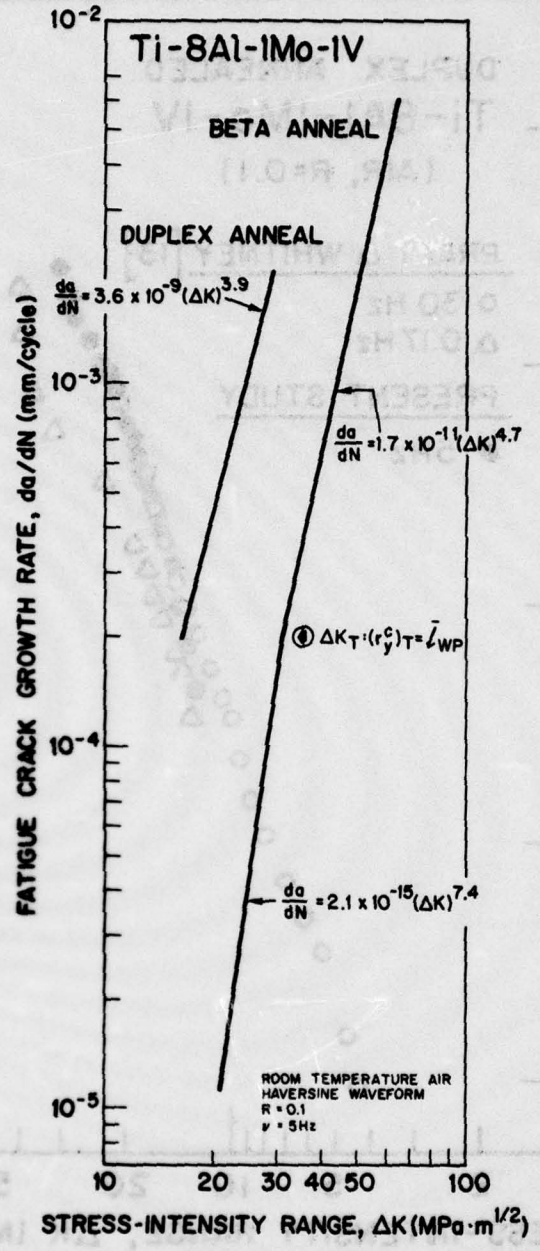

Fig. 7 — Power law characterization of fatigue crack growth behavior associated with duplex- and beta-annealed microstructures. Note the bilinear form of the growth-rate curve for the beta anneal, with a transition point at $\Delta K_T \approx 31$ MPa.m$^{1/2}$.

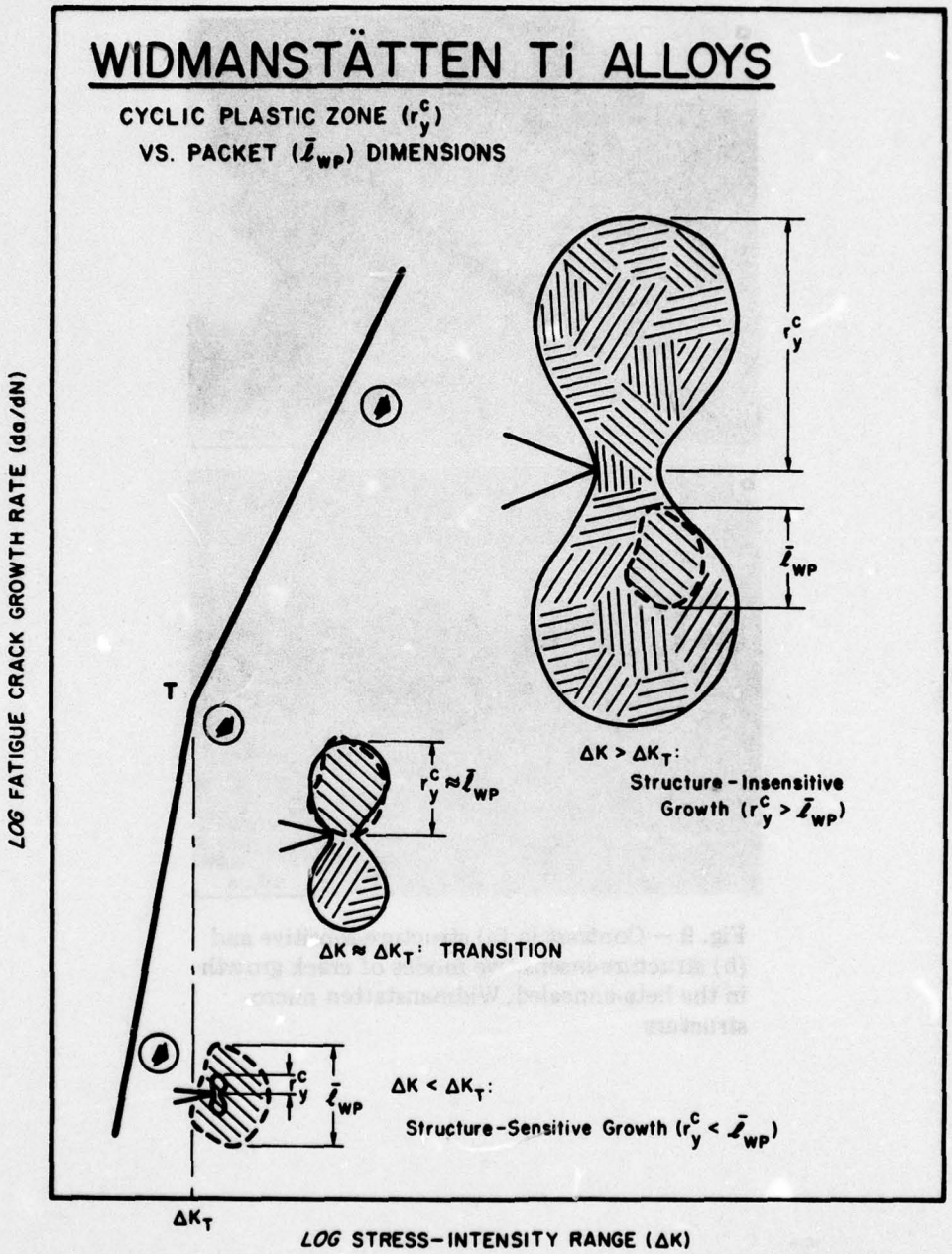

Fig. 8 — Influence of cyclic plastic zone size, relative to mean packet size, upon the development of bilinear form of fatigue crack growth behavior (cf. text)

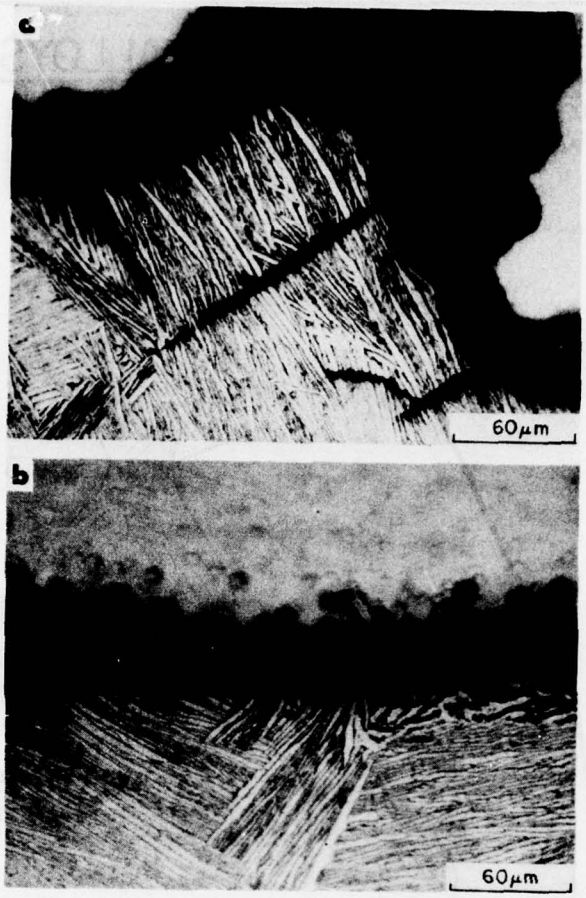

Fig. 9 — Contrast in (a) structure-sensitive and (b) structure-insensitive modes of crack growth in the beta-annealed, Widmanstätten microstructure

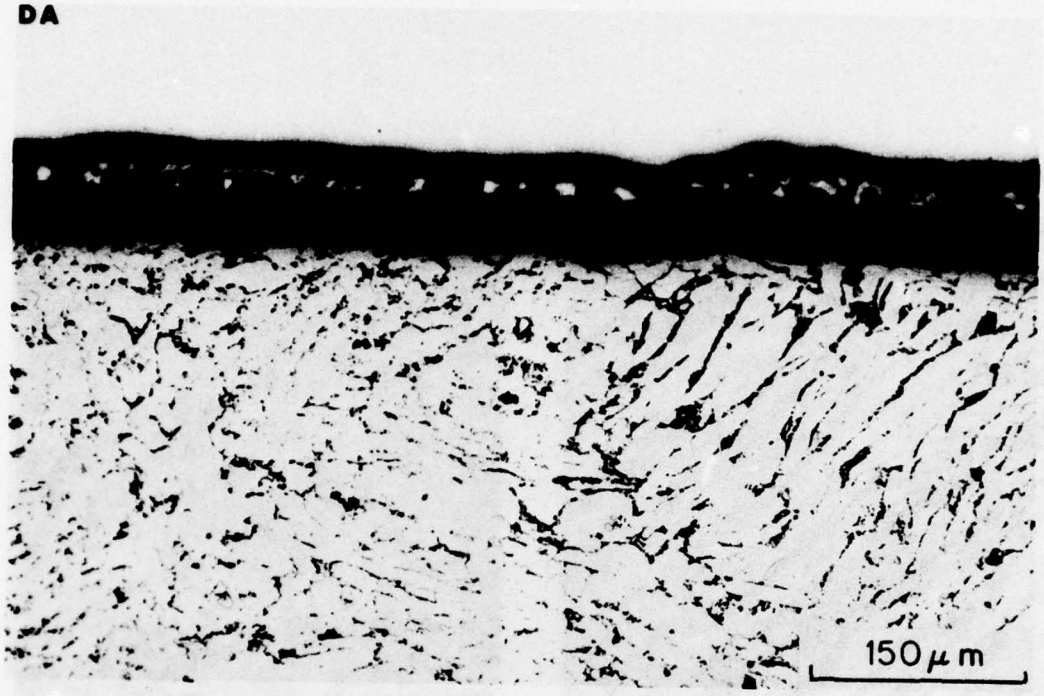

Fig. 10 — Structure-insensitive mode of fatigue crack growth in the duplex-annealed microstructure

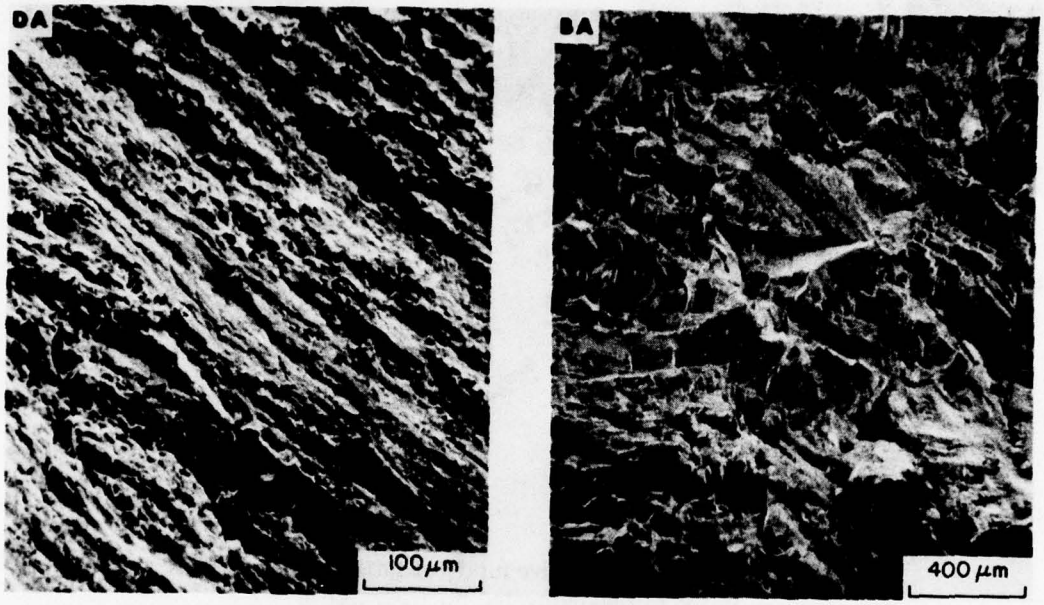

Fig. 11 — Scanning electron micrographs illustrate contrast in fracture surface topography associated with structure-insensitive growth in the duplex-annealed microstructure (DA) to structure-sensitive fatigue crack growth in the beta-annealed microstructure (BA).

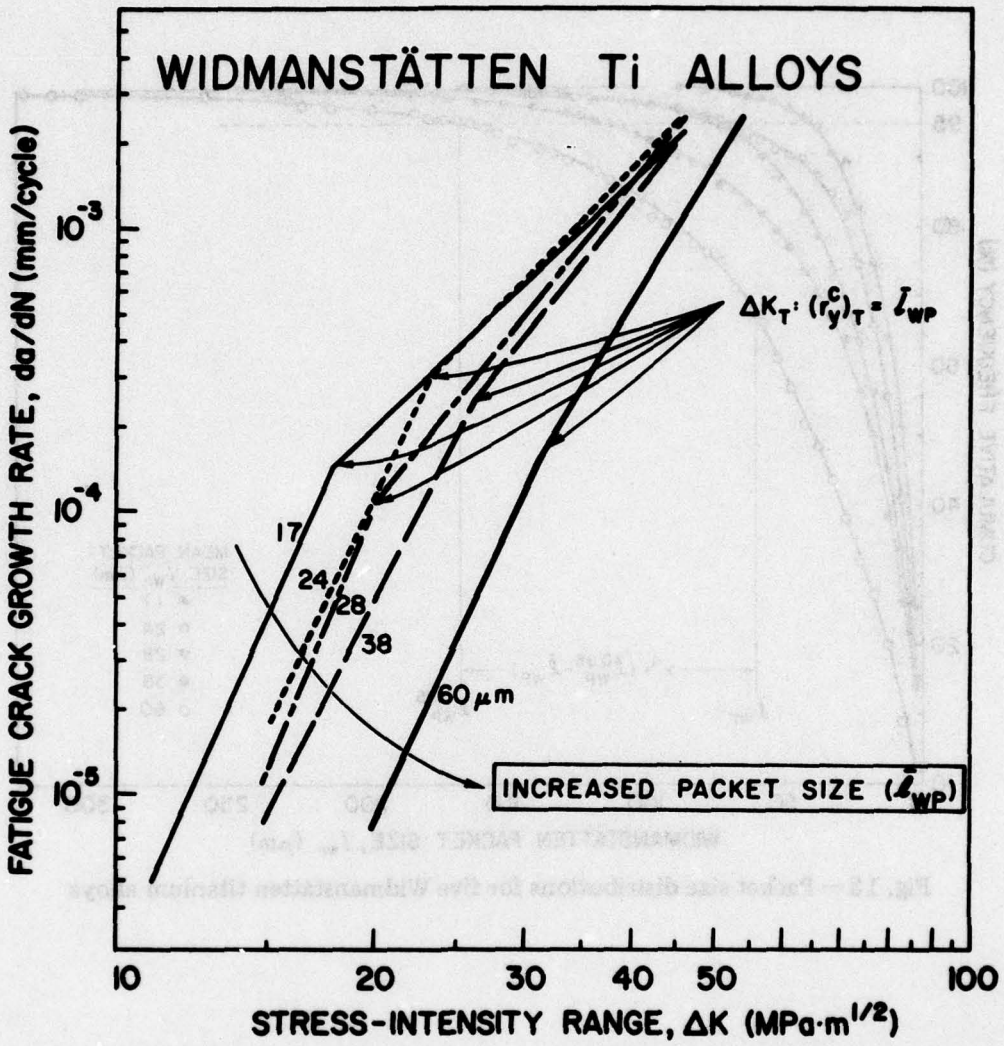

Fig. 12 — Decrease in fatigue crack growth rates with increased mean Widmanstätten packet size in beta-annealed titanium alloys

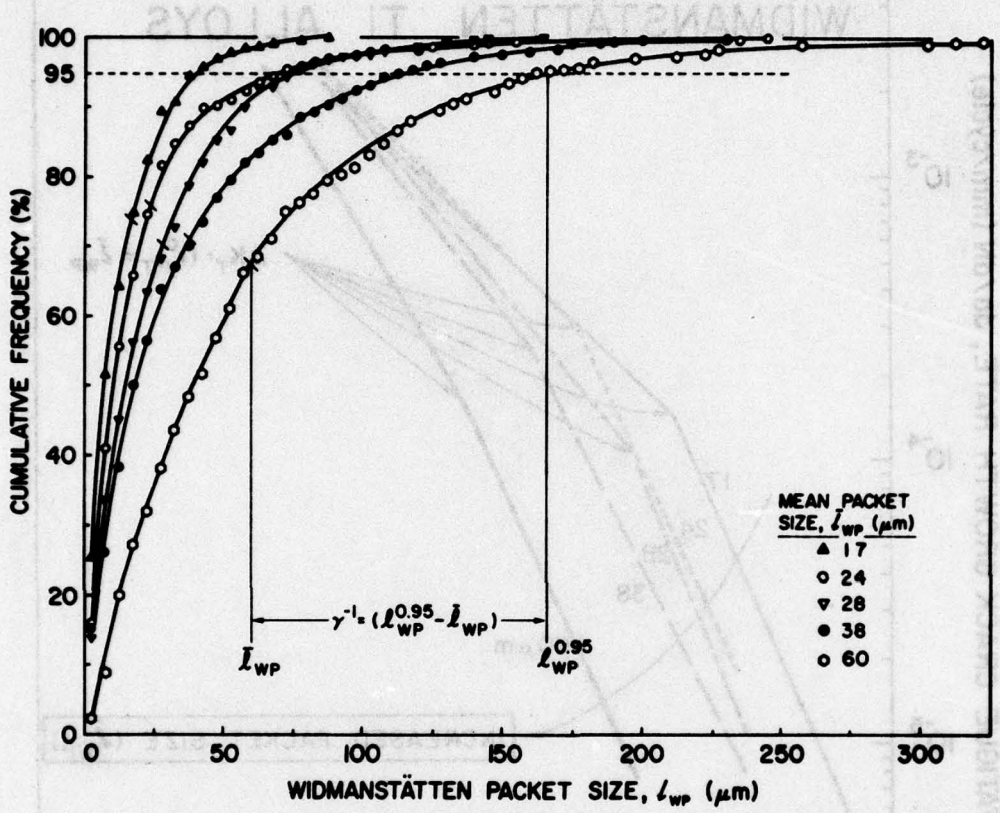

Fig. 13 — Packet size distributions for five Widmanstätten titanium alloys

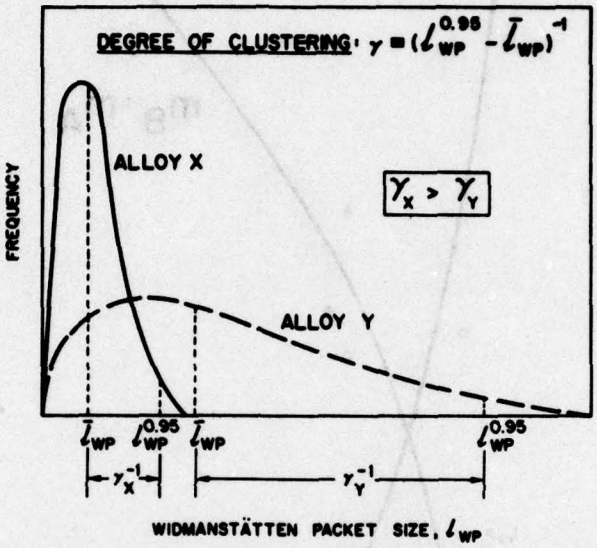

Fig. 14 — Schematic: Packet size distribution for alloy X exhibits greater clustering than for alloy Y

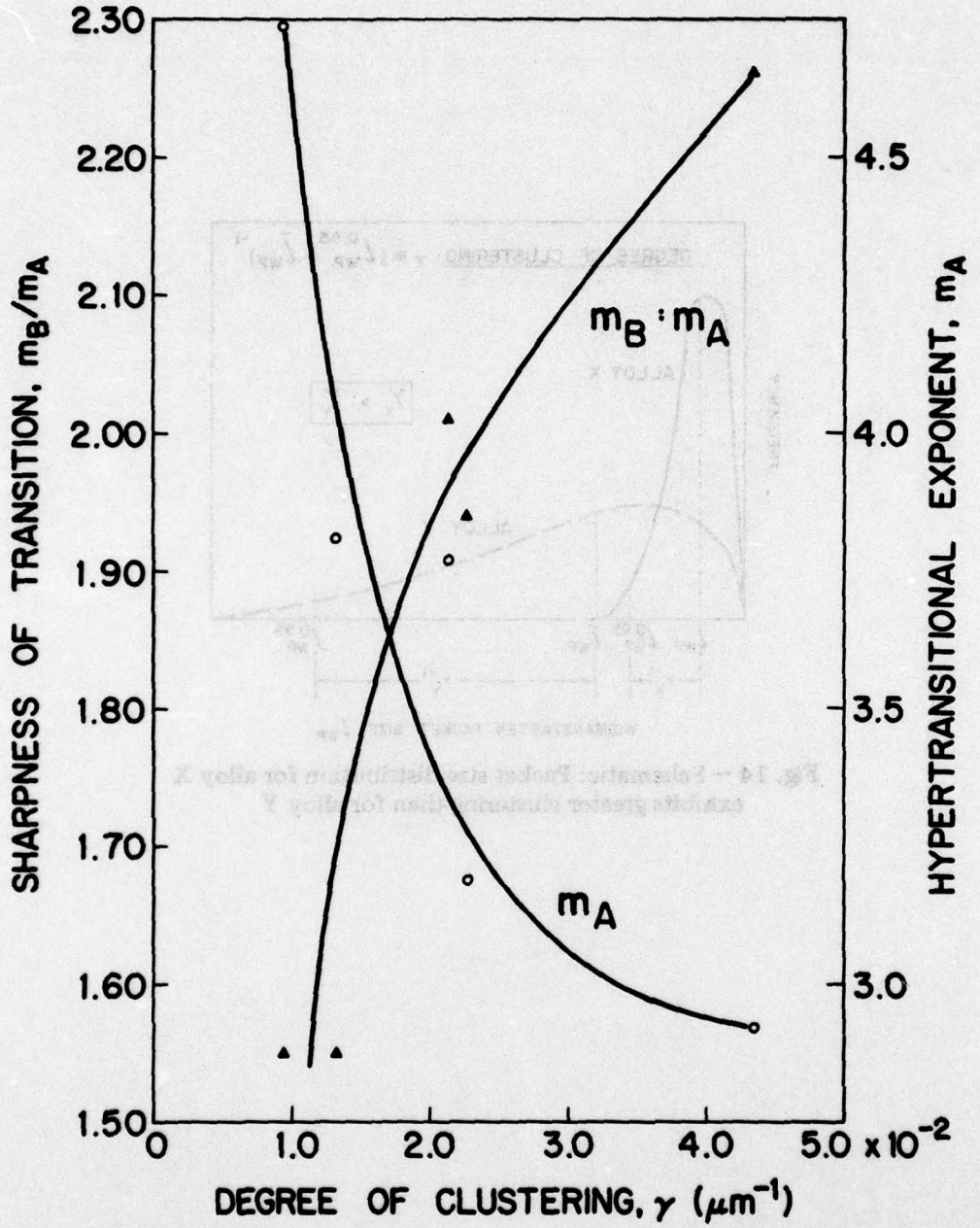

Fig. 15 — Sharpness of transition (m_B:m_A) and hypertransitional exponent (m_A) as functions of degree of clustering (γ)

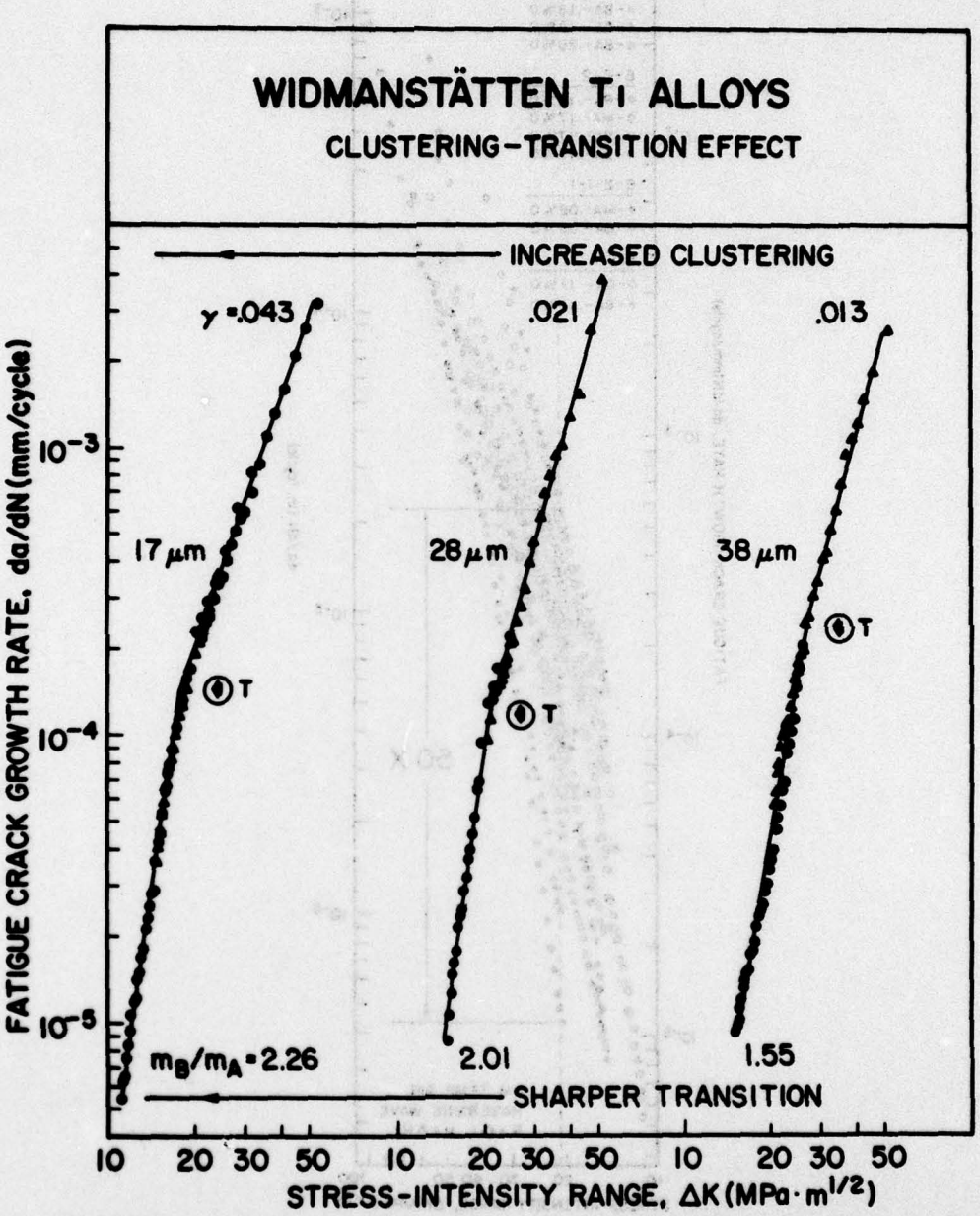

Fig. 16 — Influence of clustering on sharpness of transition observed in three logarithmic da/dN vs. ΔK data plots

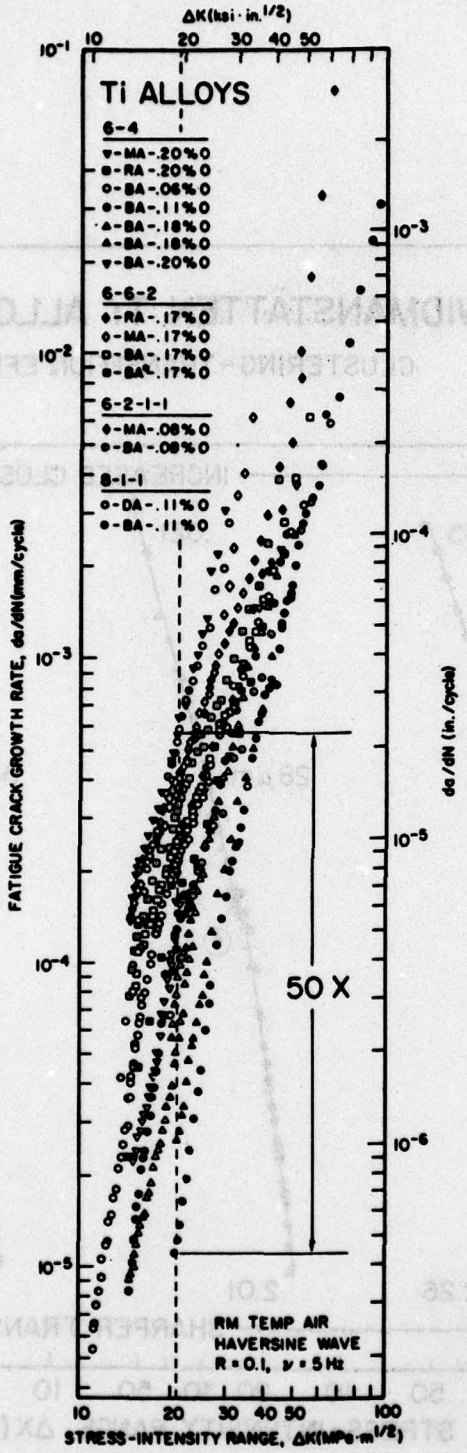

Fig. 17 — Fatigue crack growth rates for a wide variety of materials from four $\alpha + \beta$ titanium alloy systems. Note 50-fold difference in growth rates for different materials at $\Delta K = 21$ MPa·m$^{1/2}$

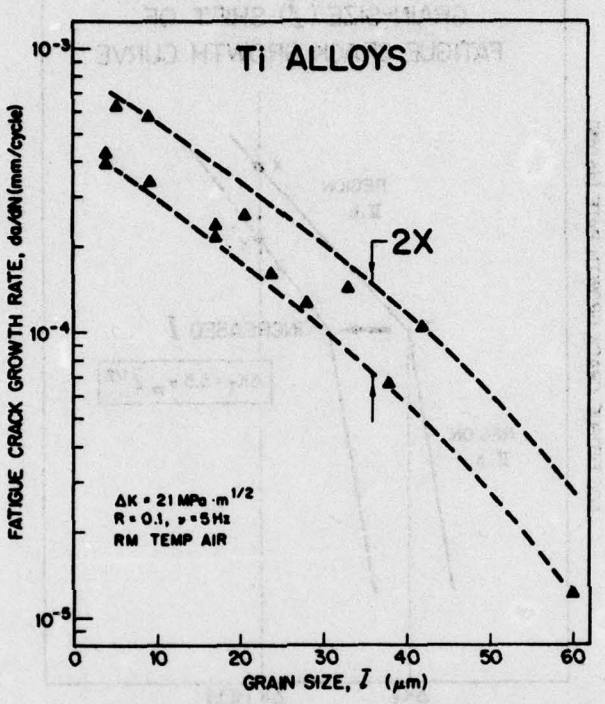

Fig. 18 — Fatigue crack growth rates for materials (in Fig. 2) at $\Delta K = 21$ MPa·m$^{1/2}$, plotted as a function of mean grain size. Note suggested narrowness of data band, 2-fold wide in da/dN.

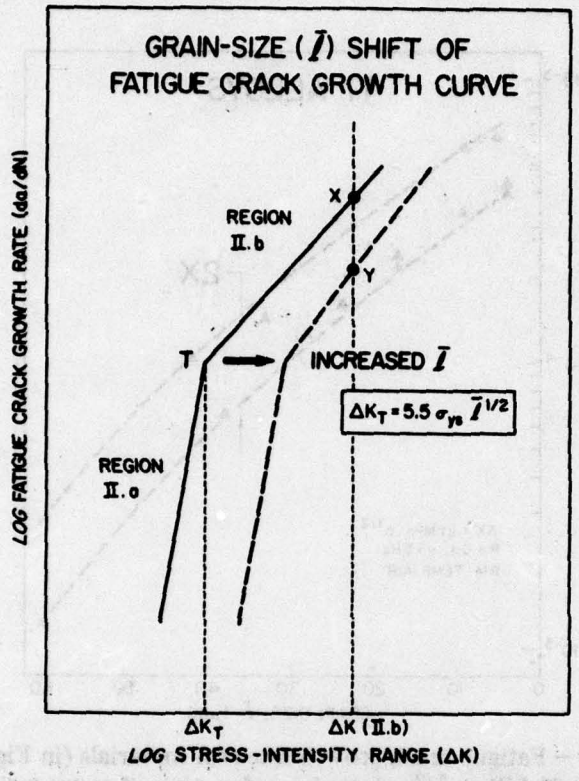

Fig. 19 — Grain-size shift of bilinear fatigue crack growth rate plot, as anticipated from reversed (cyclic) plastic zone size model. Transition from microstructurally sensitive mode of crack growth in region II.a to structure-insensitive mode in region II.b occurs at ΔK_T, where reversed plastic zone attains mean grain size. Shift in ΔK_T is predicted by Eq. (6); cf. text.

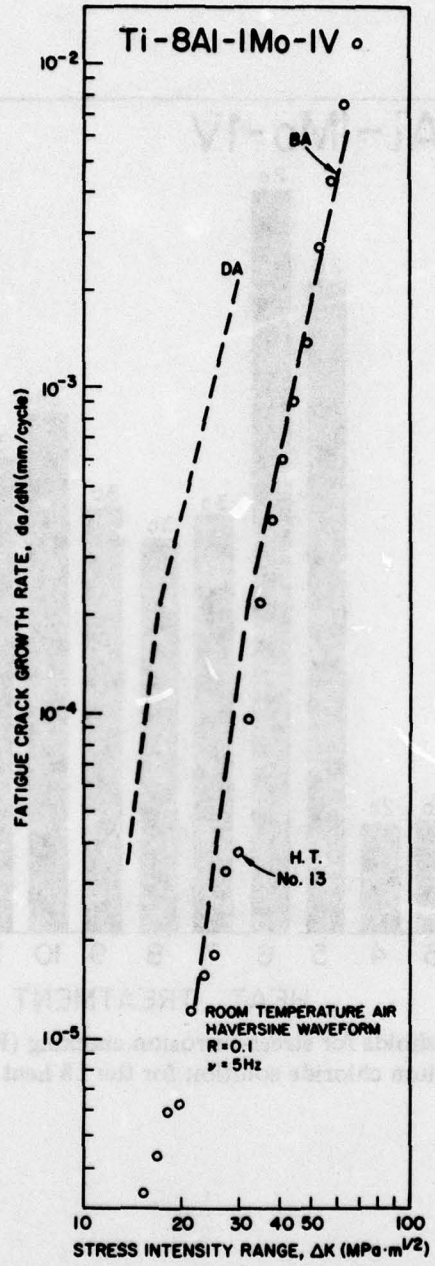

Fig. 20 — Fatigue crack growth rates for heat treatment no. 13

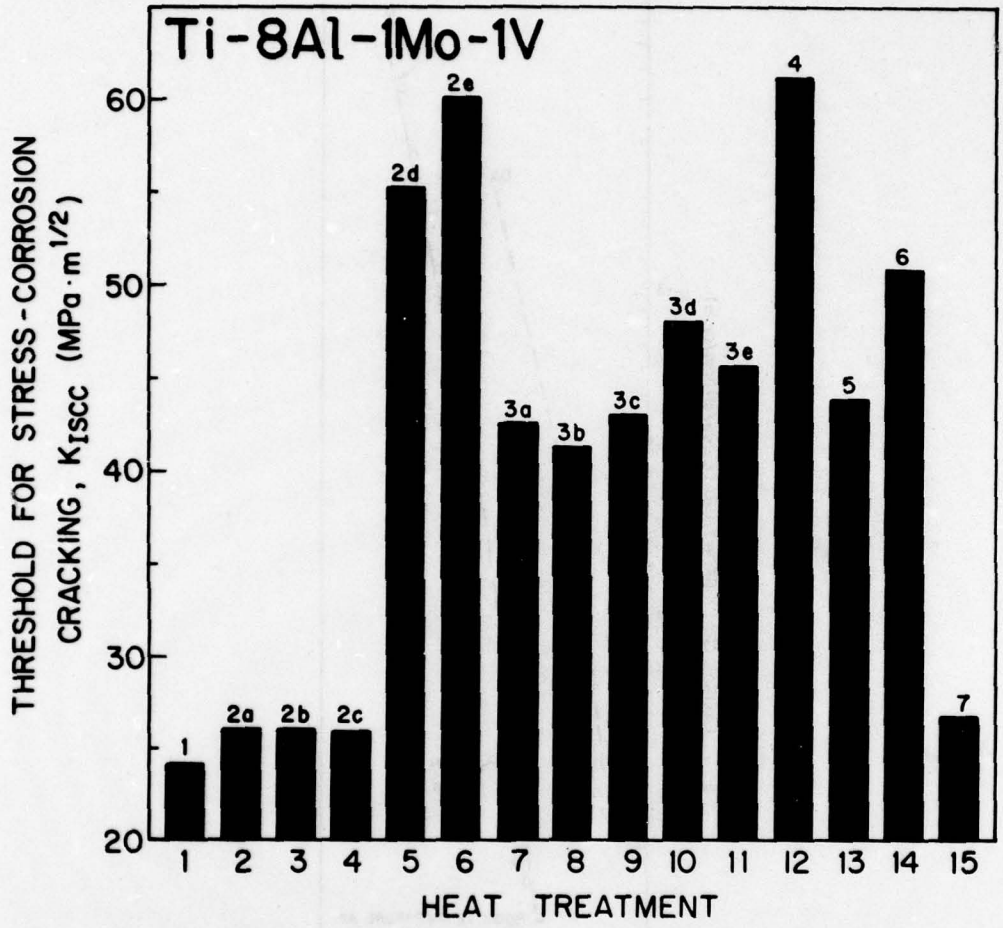

Fig. 21 — Thresholds for stress-corrosion cracking (K_{Iscc}) in 3.5% aqueous sodium chloride solution for the 15 heat treatments

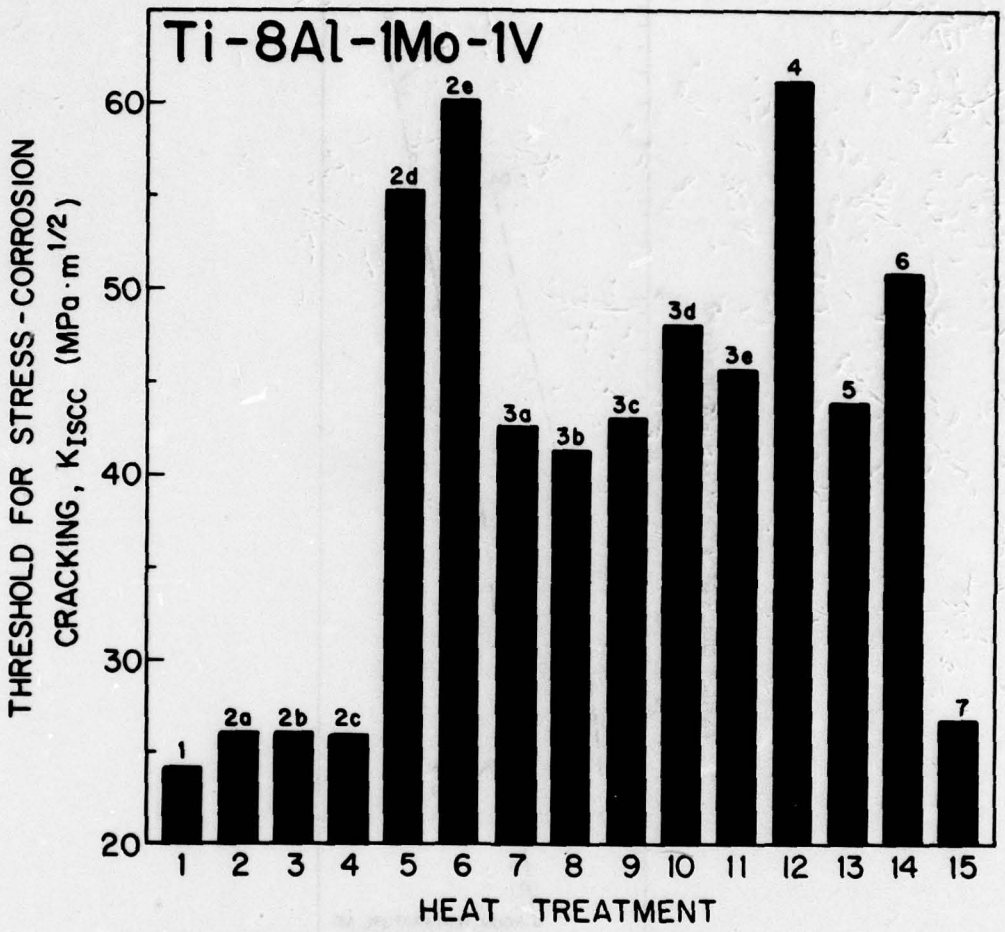

Fig. 21 — Thresholds for stress-corrosion cracking (K_{Iscc}) in 3.5% aqueous sodium chloride solution for the 15 heat treatments

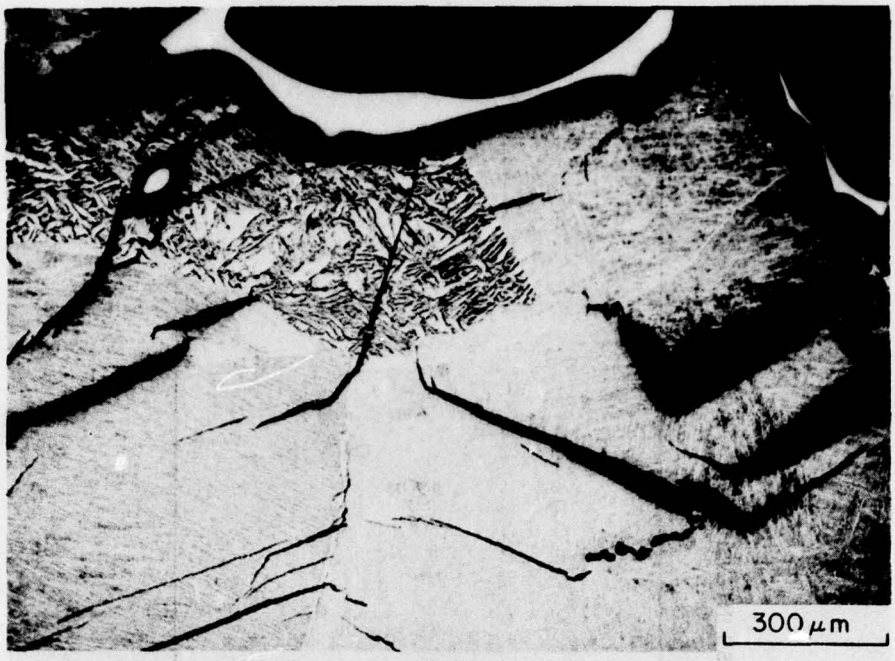

BA

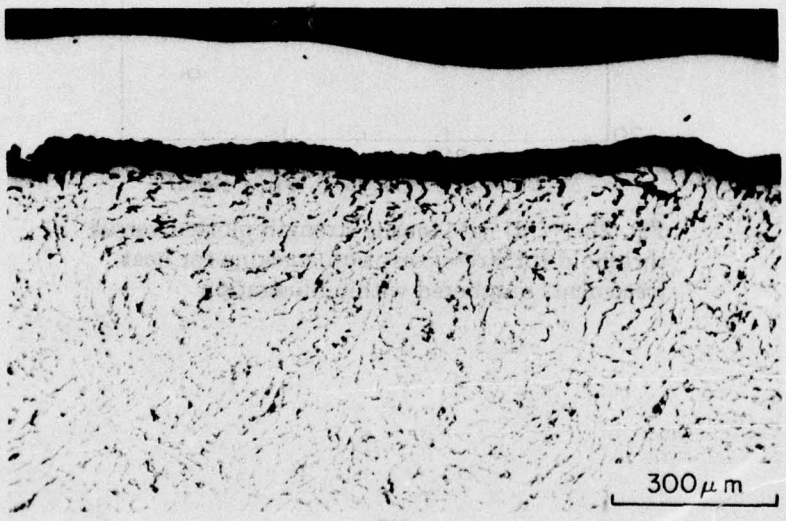

DA

Fig. 22 — Contrast in metallographic crack-path sections for stress-corrosion cracking in the beta-annealed (BA) and duplex-annealed (DA) microstructures

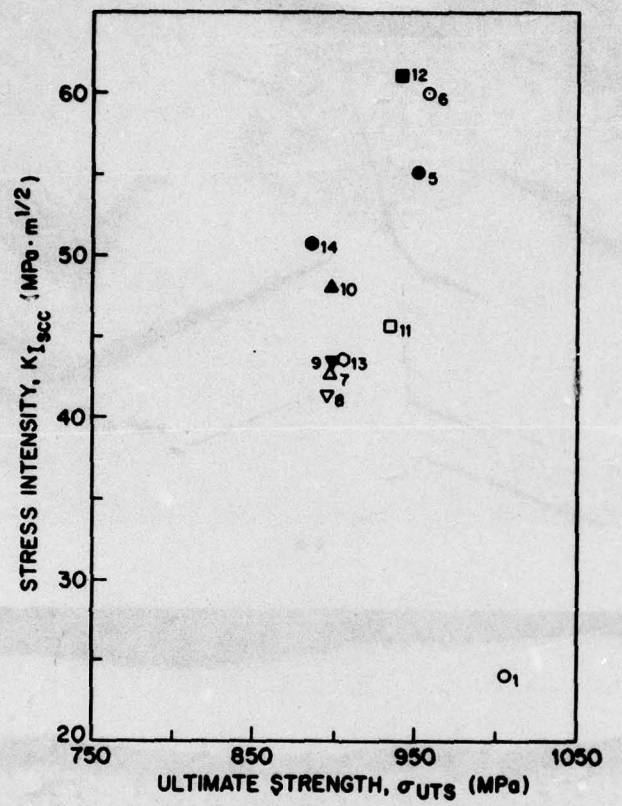

Fig. 23 — Ultimate tensile strength plotted versus threshold for stress-corrosion cracking for heat treatments numbered within illustration

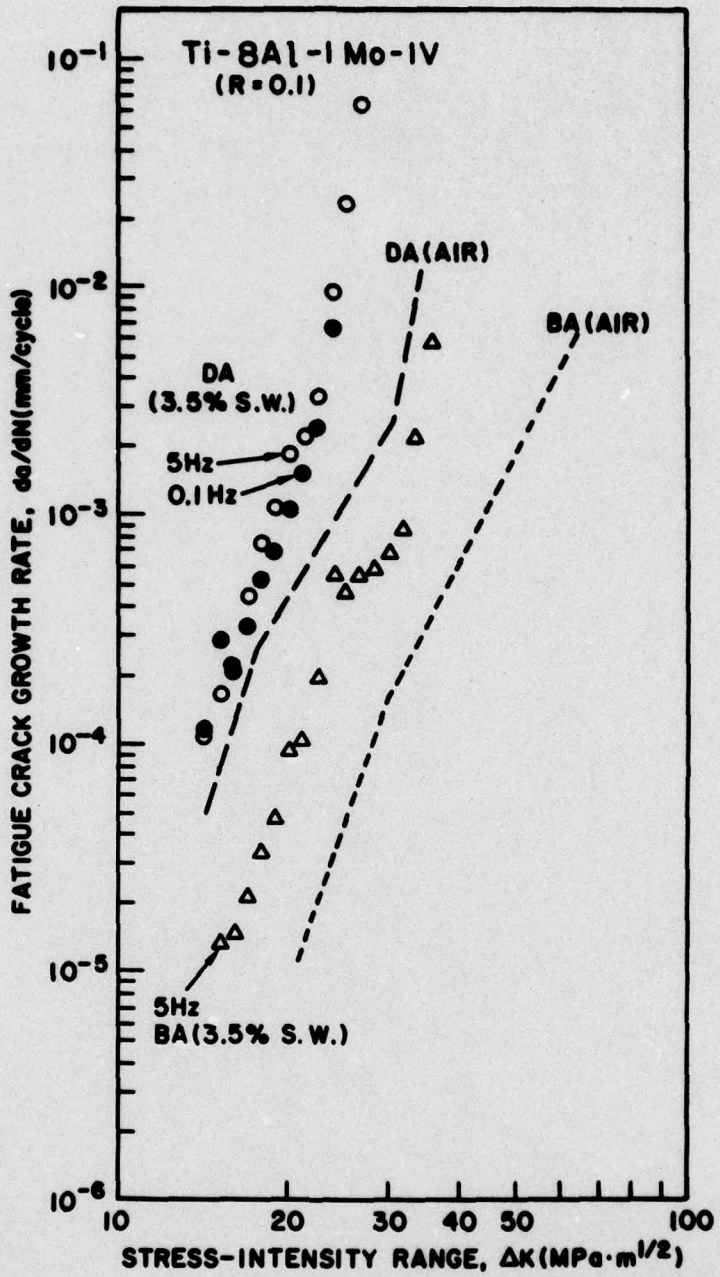

Fig. 24 — Corrosion fatigue crack growth rates in 3.5% aqueous sodium chloride solution for the duplex-annealed (DA) and beta-annealed (BA) microstructures. Data trend lines (dashed) for the respective microstructures are shown for growth rates in ambient air.

DEPARTMENT OF THE NAVY

NAVAL RESEARCH LABORATORY
Washington, D.C. 20375

OFFICIAL BUSINESS
PENALTY FOR PRIVATE USE, $300
Third Class Mail

POSTAGE AND FEES PAID
DEPARTMENT OF THE NAVY
DoD-316